# Field-dependent charge transport in organic thin-film transistors: Impact of device structure and organic semiconductor microstructure

Cite as: Appl. Phys. Lett. **115**, 073301 (2019); https://doi.org/10.1063/1.5099388 Submitted: 09 April 2019 . Accepted: 23 July 2019 . Published Online: 12 August 2019

Sajant Anand (10), Katelyn P. Goetz (10), Zachary A. Lamport (10), Andrew M. Zeidell, and Oana D. Jurchescu







# ARTICLES YOU MAY BE INTERESTED IN

Tutorial: Organic field-effect transistors: Materials, structure and operation Journal of Applied Physics 124, 071101 (2018); https://doi.org/10.1063/1.5042255

Negative differential resistance and multilevel resistive switching in BaSrTiO<sub>3</sub> films Applied Physics Letters 115, 072101 (2019); https://doi.org/10.1063/1.5113883

Low-latency adiabatic superconductor logic using delay-line clocking Applied Physics Letters 115, 072601 (2019); https://doi.org/10.1063/1.5111599









# Field-dependent charge transport in organic thin-film transistors: Impact of device structure and organic semiconductor microstructure

Cite as: Appl. Phys. Lett. 115, 073301 (2019); doi: 10.1063/1.5099388 Submitted: 9 April 2019 · Accepted: 23 July 2019 · Published Online: 12 August 2019







Sajant Anand, 🕩 Katelyn P. Goetz, 🗀 Zachary A. Lamport, 🕩 Andrew M. Zeidell, and Oana D. Jurchescu 🗀 🕞



# **AFFILIATIONS**

Department of Physics and Center for Functional Materials, Wake Forest University, Winston-Salem, North Carolina 27109, USA  $^2$ Kirchhoff Institute of Physics and Center for Advanced Materials, Universität Heidelberg, 69120 Heidelberg, Germany

### **ABSTRACT**

Organic semiconductors are highly susceptible to defect formation, leading to electronic states in the gap—traps—which typically reduce the performance and stability of devices. To study these effects, we tuned the degree of charge trapping in organic thin-film transistors by modifying the film deposition procedures and device structure. The resulting charge carrier mobility varied between 10<sup>-3</sup> and 10 cm<sup>2</sup>/V s in 2,8-difluoro-5,11-bis(triethylsilylethynyl)anthradithiophene. We analyzed the data using a Poole-Frenkel-like model and found a strong dependence of mobility on the field in low-mobility transistors and a field-independent mobility in high-performance devices. We confirmed the presence of traps in all films investigated in this study and concluded that the Poole-Frenkel model is not sufficiently sensitive to identify traps when their concentration is below the detection limit.

Published under license by AIP Publishing. https://doi.org/10.1063/1.5099388

Organic semiconductors have sparked interest owing to their ease of processing, chemical versatility, and tunable properties, which establishes them as viable candidates for incorporation in large-area, flexible, and bendable electronic applications. The weak nature of the bonding energies within the organic solids is key to their processing: organic semiconductors can be deposited at or close to room temperature from solutions or by laser printing.<sup>1-3</sup> Such manufacturing processes are both low-cost and compatible with flexible substrates. On the other hand, the weak intermolecular interactions make these semiconductors less resistant to defect formation, which often leads to the creation of electronic traps. 4-6 The presence of trap states lowers the performance and stability of electronic devices.<sup>7,8</sup> A thorough understanding of the generation of traps in organic semiconductors and their impact on charge transport is therefore critical for these materials to realize their robust industrial prospects. Numerous methods have been proposed for the investigation of electronic traps in organic semiconductors. 4,9,10

We address this topic by using organic thin-film transistor (OTFT) devices. We varied the trap density by tuning the semiconductor film microstructure, device structure, and device composition and evaluated the dependence of the charge-carrier mobility on the longitudinal electric field (i.e., determined by the drain-source voltage) using a Poole-Frenkel-like analysis. Such field-dependent transport was previously observed in both polymeric and small-molecule organic semiconductors and has been assigned to the presence of disorder at the grain boundaries and interface states. 11-18 Here, we report on a transition from a pronounced dependence of the mobility on the electric field to a field-independent mobility as the density of grain boundaries and density of interface states decrease. We found that the Poole-Frenkel model cannot detect the presence of the traps in the semiconductor layer when their density is low and concluded that this model has limited applicability in organic semiconductors characterized by a small defect density.

The devices used in this study are a combination of the bottomgate (BG), bottom-contact, coplanar structure [Fig. 1(a)] and the topgate (TG), bottom-contact, staggered structure [Fig. 1(b)]. Coupled with the optional deposition of a pentafluorobenzene thiol (PFBT) selfassembled monolayer (SAM) on the surface of the source and drain electrodes, in total, four different device types have been fabricated. A summary of device structures is included in Table I. Type 1 OTFTs correspond to the structure in Fig. 1(a) and consist of a SiO<sub>2</sub> dielectric and untreated Au electrodes. Type 2 devices are similar, with the exception that a PFBT treatment was applied to the contacts prior to the organic semiconductor deposition. For type 3 and type 4 samples, the structure

a) jurchescu@wfu.edu

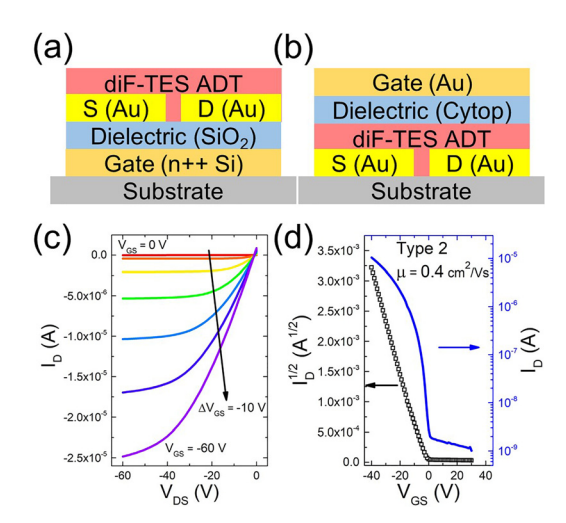


**FIG. 1.** OTFT device structures and current-voltage characteristics of a type 2 device: (a) bottom-gate, bottom-contact, coplanar structure; (b) top-gate, bottom-contact, staggered structure. (c) Evolution of drain current ( $I_D$ ) with drain-source voltage ( $V_{DS}$ ) for fixed source-gate voltages  $V_{GS}=0 \rightarrow -60 \, \text{V}$ , in steps of  $-10 \, \text{V}$ . (d) Evolution of  $I_D$  with  $V_{GS}$  for fixed  $V_{DS}$ ; left axis:  $\sqrt{I_D}$  vs  $V_{GS}$ ; right axis:  $\log (I_D)$  vs  $V_{GS}$ .

in Fig. 1(b) was adopted, with a Cytop dielectric and Au or PFBT/Au contacts, respectively. By varying the device architecture and details of fabrication, we tuned the charge carrier mobility by almost four orders of magnitude, from 0.004 to 7.7 cm<sup>2</sup>/V s, in 2,8-difluoro-5,11-bis(triethylsilylethynyl)anthradithiophene (diF-TES ADT). The highest mobility obtained in our devices is on par with the best values reported on this material.<sup>19–21</sup> We note that higher mobilities can be obtained by aggressively reducing the contact resistance<sup>22</sup> and by incorporating dopants which play a dual role in optimizing the film microstructure and lowering the injection barrier.<sup>23</sup>

The OTFTs were fabricated following the process reported elsewhere.  $^{22,24,25}$  We started with a highly-doped silicon wafer with a 200 nm thermally grown SiO<sub>2</sub> layer on its surface. This simultaneously served as the bottom-gate electrode and dielectric for type 1 and 2 devices. Following a standard substrate cleaning step, source and drain contacts (5 nm Ti/40 nm of Au) were deposited. Channel lengths ranged from  $L=30~\mu{\rm m}$  to  $100~\mu{\rm m}$ . For type 2 and 4 devices, PFBT treatment was performed. This treatment has been shown to modify

**TABLE I.** Summary of device parameters. To calculate the average mobility, all measurements were taken at  $V_{\rm DS}=-40\,{\rm V}$ . For  $\gamma$  and  $\mu_0$  of type 2 and 3 devices, the first row is the low electric field regime, and the second is the high electric field regime.

Туре	Contacts	Dielectric	$\mu_{\text{avg}}$ (cm <sup>2</sup> /Vs)	$(m^{1/2}/V^{1/2})$	$\mu_0$ (cm <sup>2</sup> /Vs)
1	Au	BG (SiO <sub>2</sub> )	0.006	0.0030	0.001
2	PFBT/Au	BG (SiO <sub>2</sub> )	0.22	0.0026	0.02
				$9.0 \times 10^{-4}$	0.08
3	Au	TG (Cytop)	0.05	0.0025	0.007
				0.0011	0.01
4	PFBT/Au	TG (Cytop)	2.9	$6.5 \times 10^{-4}$	1.6

the diF-TES ADT film microstructure and reduce the contact resistance by increasing the electrode work function.  $^{26,27}$  The organic semiconductor layer was deposited by spin coating from a 1.5 wt. % solution in chlorobenzene. For the type 3 and 4 devices, a layer of Cytop deposited by spin-coating acted as a top-gate dielectric. The final step in the fabrication of type 3 and 4 devices was the evaporation of a 20 nm Au top-gate electrode.

The OTFTs were characterized first at room temperature in a nitrogen environment, and the mobility  $\mu$  was extracted in the saturation regime.  $^{28}$  We evaluated the mobility at different source-drain voltages ( $V_{\rm DS}$ ), while ensuring that the device was in the saturation regime. The evolution of the mobility with temperature was evaluated in a vacuum probe station in the temperature range of  $200\,{\rm K} < {\rm T} < 300\,{\rm K}$ . This rather limited temperature interval was chosen in order to avoid the effects of structural phase transitions present in diF-TES ADT.  $^{29}$  A cool/heat ramp of 0.5 K/min was chosen in order to avoid film degradation due to temperature induced strain at device interfaces.  $^{25,30}$  The activation energy was determined by an Arrhenius-like relation.

In Figs. 1(c) and 1(d), we provide an example of current-voltage characteristics for type 2 devices. Examples of the other types are provided in Figs. S1–S3 in the supplementary material. Figure 1(c) shows the dependence of the drain current ( $I_{\rm D}$ ) on  $V_{\rm DS}$  for several constant source-gate voltages ( $V_{\rm GS}$ ). Figure 1(d) shows the dependence of  $I_{\rm D}$  on  $V_{\rm GS}$  at constant source-drain voltage,  $V_{\rm DS}=-40\,{\rm V}$ . On the left axis, in open black squares, the linear dependence of  $\sqrt{I_{\rm D}}$  on the source-gate voltage  $V_{\rm GS}$  confirms the validity of the gradual channel approximation in our devices and the value of the saturation mobility  $\mu_{\rm sat}$  extracted from transfer measurements.

At least 30 devices of each type, resulting from multiple independent fabrications following identical procedures, were measured and analyzed. The average values of  $\mu$  obtained for each device type at  $V_{\rm DS}$  $= -40 \,\mathrm{V}$  are listed in Table I. The significant variation in mobility for the four sample types, which occurs in spite of the fact that the same organic semiconductor was used, originates from the differences in contact resistance and trap densities at the semiconductor/dielectric interfaces, as well as the modifications in the semiconductor microstructure, as we have shown in our previous work.<sup>24,27</sup> In short, a lower contact resistance for the FETs with PFBT-modified contacts allows for more efficient charge injection, and the polymer dielectric Cytop provides a low interfacial trap density.<sup>24</sup> The values for the contact resistance, as estimated by the gated transmission line method,<sup>28</sup> are as follows:  $R_CW = 587 \text{ k}\Omega$  cm for type 1 devices,  $R_CW = 6.7 \text{ k}\Omega$ cm for type 2,  $R_CW = 80 \text{ k}\Omega$  cm for type 3, and  $R_CW = 960 \Omega$  cm for type 4. In addition to causing a shift in the electrode work function, the PFBT treatment modifies the film microstructure to enhance charge transport. While devices with untreated contacts (types 1 and 3) consist of films of small grains of mixed "face-on" and "edge-on" molecular orientation, in devices with treated contacts (types 2 and 4), the semiconductor film adopts a preferential orientation of the diF-TES ADT molecules along the high-mobility edge-on (001) direction. This also leads to the formation of large grains within the semiconductor films, i.e., a low density of grain boundaries.<sup>27</sup> The ability to tune the device properties via fabrication provides a platform for the study of charge transport in different trapping regimes with no modifications in the chemical structure of the organic semiconductor.

To understand the impact of traps and disorder on charge transport, we measured the dependence of mobility on the lateral electric field and analyzed the measurements using a Poole-Frenkel-like model. In its original context, the Poole-Frenkel detrapping model describes an increase in conductivity at a rate proportional to  $\exp\sqrt{E}$ : an increasing field reduces the Coulomb potential energy barrier of a trap state (explicitly, a trap state that is charged when empty) allowing more charges to escape through thermal excitations and contribute to the current. A similar increase in mobility has also been observed due to static disorder, which causes broadening of the density of states (DOS) near the transport band. Although in our case the physics is quite different from the original model, it shows the same trend, and we will refer to the analysis as a "Poole-Frenkel-like model." The effective mobility  $\mu$  is given by the following equation:

$$\mu = \mu_0 \exp\left(\gamma \sqrt{E}\right),\tag{1}$$

where  $\mu_0$  is the zero-field mobility, E is the electric field, and  $\gamma$  is the Poole-Frenkel coefficient. In Fig. 2, we plot the mobility vs  $\sqrt{E}$  for one device of each type. We determined E as the ratio between  $V_{DS}$  and L. Numerical simulations and experimental results have proven that this assumption is valid even for the case of OTFTs operating in the saturation regime. 11,32,33 The linear dependence of  $\log (\mu)$  on  $\sqrt{E}$  is in agreement with the Poole-Frenkel model described in Eq. (1). Severe contact effects, however, may lead to a similar outcome, since increasing the applied bias reduces the potential energy barrier (Schottky barrier) at the metal/organic semiconductor interface. While we do not exclude the contributions of contacts, our previous studies confirm that all four device types are not severely limited by the contacts. 26,27 The slopes of the linear fits to these curves give the cofactor  $\gamma$ , while the intercept with the mobility axis provides  $\mu_0$ . The values extracted for the four device types are included in Table I. The strong dependence of mobility on the field found in type 1 devices (black squares),  $\gamma \approx 10^{-3}$ , indicates the presence of a high density of traps and structural disorder and results in a low mobility. The structural disorder arises from the large grain boundary density [Fig. 3(a) (inset)] and misalignment of grains resulting from the extrinsic processing conditions, while electronic traps arise from bulk effects and the scattering at the interface with the SiO<sub>2</sub> dielectric.<sup>34</sup> This scattering originates

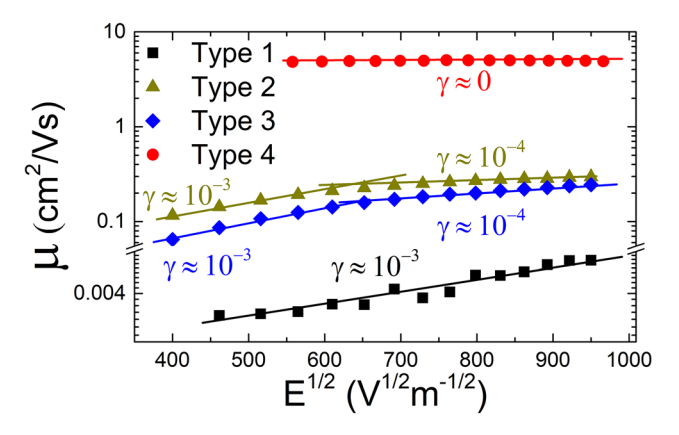


**FIG. 2.** Mobility  $\mu$  vs  $\sqrt{E}$  (log-linear scale) for each device type showing one regime for type 1 and 4 devices and two regimes for both the type 2 and 3 devices.

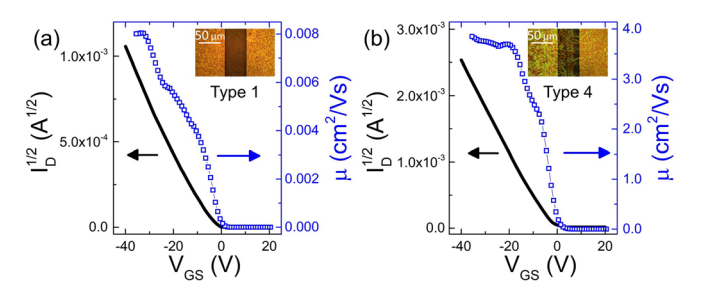


**FIG. 3.** Mobility (right axis, open blue squares)  $\mu$  and the square root of the drain current (left axis, black line)  $I_{\rm D}$  vs  $V_{\rm GS}$  for (a) type 1 and (b) type 4 devices. The insets show optical micrographs of the devices. The film denoted here as type 1 is identical to the film in type 3 devices, while the films in type 2 and type 4 devices are identical as well.

from the dangling hydroxyl groups<sup>35</sup> and Fröhlich polarons<sup>36</sup> present here, as well as the strain due to mismatch in the thermal expansion of consecutive device layers.<sup>25</sup> In addition, it was shown that the lateral electric field can be inhomogeneous in polycrystalline films, where a strong effective local field forms at the grain boundaries. This electric field confinement effect leads to the creation of domains where the field is much higher than the average, thus dominating the transport.<sup>37</sup> On the contrary, the type 4 device (red circles) exhibits a mobility that is independent of the applied field, with  $\gamma \approx 0$ , suggesting that a trap-free regime was reached. Here, the grain size is significantly larger [Fig. 3(b) (inset)], and the scattering at the interface with the dielectric is low. Type 2 devices (gold triangles) are characterized by a considerable field dependence  $(\gamma \approx 10^{-4} - 10^{-3})$ , in spite of the fact that the grain size is similar to that in type 4 devices due to the presence of PFBT treatment [Fig. 3(b) (inset)]. The enhanced trapping is the result of the processes occurring at the SiO<sub>2</sub> surface, as described earlier. The organic semiconductor film in type 3 devices (Fig. 2 blue diamonds) benefits from reduced trapping at the Cytop surface, but the large density of grain boundaries is responsible for the pronounced dependence of the mobility on field. For type 2 and 3 devices, the Poole-Frenkel graph exhibits two regimes: at low E,  $\mu$ increases abruptly with the increasing electric field, and a large value of  $\gamma$ is recorded, similar to that in the type 1 devices. At larger fields, the energetic barriers are reduced such that the probability for the charges to escape the trap increases, and the device transitions into a state characterized by a lower trap density and a milder dependence of  $\mu$  on the field.

The values of  $\gamma$  recorded in type 1, 2, and 3 devices are similar to those reported in similar organic semiconductors. 12,14,18 The question is whether type 4 devices are indeed "trap-free" or the Poole-Frenkeltype analysis is unable to detect the presence of traps. To gain a deeper understanding of the energetic landscape of the electronic traps in our devices, we performed a spectral analysis of the trap density of states (DOS); the results are illustrated in Fig. S4, supplementary material. It can be clearly observed that the DOS shows an exponential valence band tail in the bandgap<sup>38</sup> and that the devices fabricated at the surface of SiO<sub>2</sub> dielectric have significantly larger trap densities than those on Cytop. The electronic states present in the forbidden gap can be in the form of shallow traps (due to structural disorder at grain boundaries, roughness, or strain at the semiconductor/dielectric interface)<sup>25,26</sup> or deep traps (isomer coexistence), 39,40 and these states are clearly detected even in type 4 devices. These results seem to contradict the outcome of the Poole-Frenkel analysis, in which the invariance of the

mobility with the longitudinal electric field points to a trap-free system. We suggest that when the density of trap states in a device is very low, such as in the case of type 4 OTFTs, the Poole-Frenkel-type analysis is unable to provide information about the trapping states in the semiconductor layer. In this case, the models that take into account the dependence of mobility on the charge-carrier concentration are more appropriate to describe the effect of disorder on charge transport. Al -43 These models predict no field dependence in this field range at room temperature, whereas at higher fields and/or low temperature, the field effect on transport becomes relevant.

The presence of traps also results in a distinct dependence of the mobility on  $V_{\rm GS}$  and temperature. Therefore, we focus on the study of charge transport as a function of these two variables in the next section. In Figs. 3(a) and 3(b), we show the evolution of mobility on  $V_{GS}$ in a device of type 1 and type 4, respectively, together with the curve of  $I_{\rm D}$  from which this mobility was extracted. The continuous increase in mobility with the applied gate voltage in Fig. 3(a) results from a large density of traps, coupled with a severe injection barrier. 44 Indeed, a Schottky injection barrier of ≈0.2 eV was found between Au and the diF-TES ADT film deposited on its surface.<sup>27</sup> The PFBT treatment shifts the Au work function, and the barrier vanishes.<sup>27</sup> It is also possible that this injection barrier contributes to an increase in the cofactor  $\gamma$  in type 1 and 4 devices. The reduction in trap densities and annihilation of the injection barrier are reflected in a sharp increase in mobility, followed by a plateau, as can be seen in Fig. 3(b). Comparing our results with numerical simulations,44 we conclude that such a dependence reveals a device with ohmic contacts and a level of disorder within the semiconductor film that affects charge transport (in a trapfree OTFT, the mobility is independent of the gate voltage). The temperature response of the mobility supports the same conclusions. The results are included in Fig. 4(a). The activation energy  $E_A$  is listed in the inset. The strong dependence of mobility on temperature in type 1 devices (black squares) is a result of the significant trapping, in agreement with the Poole-Frenkel results in Fig. 2. As the roomtemperature mobility increases ( $\mu_1 < \mu_3 < \mu_2 < \mu_4$ ), both  $\gamma$  in the Poole-Frenkel plot and E<sub>A</sub> decrease, such that the high-mobility devices (type 4) show a minimal dependence of mobility on temperature, with a very small activation energy,  $E_A = 12$  meV. Here, the trap density was below the detection limit of the Poole-Frenkel model, and we approach bandlike transport. The changes in the trap densities, N<sub>T</sub>, as a function of temperature are included in Fig. 4(b). The increase in N<sub>T</sub> with reducing temperature results from the temperature-dependence

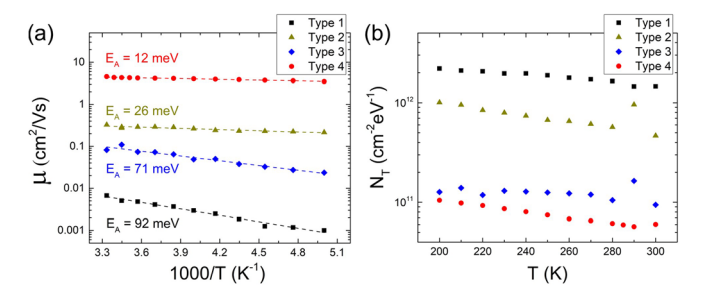


**FIG. 4.** (a) Mobility  $\mu$  vs 1000/T. The activation energy  $E_{\rm A}$  is extracted using the Arrhenius equation  $\mu \propto \exp{(-E_{\rm A}/k_{\rm B}T)}$ . (b) Interfacial trap density as a function of temperature for the four device types explored in this study. N<sub>T</sub> is extracted from the value of the threshold voltage.

of the Fermi statistics<sup>38</sup> and from the generation of traps due to strain present at the semiconductor/dielectric interface as a product of mismatch in the thermal expansion properties of the two consecutive layers.<sup>25</sup>

In summary, we have shown that the Poole-Frenkel cofactor  $\gamma$ , which quantifies the dependence of device mobility on the longitudinal electric field, can vary greatly in an OTFT depending on the device structure, device composition, and organic semiconductor film microstructure. We found that a high trap density and structural disorder in the semiconductor layer are reflected in a low mobility, which varies greatly with the applied field and a high activation energy. The cofactor  $\gamma$  is anticorrelated with mobility, and a field- and temperature-independent mobility was achieved in the highest-performing devices. Our work highlights the limitations of the Poole-Frenkel analysis in conjunction with organic transistors and emphasizes the fact that the absence of a field-dependent mobility is not always a definitive proof of the presence of a trap-free semiconductor layer.

See the supplementary material for current-voltage characteristics for type 1, 3, and 4 devices and for DOS analysis of all device types.

This work was supported by the National Science Foundation under Grant Nos. CMMI 1537080 and ECCS 1810273.

## **REFERENCES**

<sup>1</sup>W. Zhang, J. Smith, S. E. Watkins, R. Gysel, M. McGehee, A. Salleo, J. Kirkpatrick, S. Ashraf, T. Anthopoulos, M. Heeney, and I. McCulloch, J. Am. Chem. Soc. 132, 11437 (2010).

<sup>2</sup>A. C. Arias, S. E. Ready, R. Lujan, W. S. Wong, K. E. Paul, A. Salleo, M. L. Chabinyc, R. Apte, R. A. Street, Y. Wu, P. Liu, and B. Ong, Appl. Phys. Lett. 85, 3304 (2004).

<sup>3</sup>P. J. Diemer, A. F. Harper, M. R. Niazi, A. J. Petty, J. E. Anthony, A. Amassian, and O. D. Jurchescu, Adv. Mater. Technol. 2, 1700167 (2017).

<sup>4</sup>J. Dacuña and A. Salleo, Phys. Rev. B **84**, 195209 (2011).

<sup>5</sup>W. L. Kalb, S. Haas, C. Krellner, T. Mathis, and B. Batlogg, Phys. Rev. B 81, 155315 (2010).

<sup>6</sup>T. Hallam, M. Lee, N. Zhao, I. Nandhakumar, M. Kemerink, M. Heeney, I. McCulloch, and H. Sirringhaus, Phys. Rev. Lett. 103, 256803 (2009).

<sup>7</sup>A. Salleo, Organic Electronics (Wiley-VCH Verlag GmbH & Co. KGaA, Weinheim, Germany, 2013), pp. 341–380.

<sup>8</sup>A. Campos, S. Riera-Galindo, J. Puigdollers, and M. Mas-Torrent, ACS Appl. Mater. Interfaces 10, 15952 (2018).

<sup>9</sup>W. L. Kalb and B. Batlogg, Phys. Rev. B **81**, 035327 (2010).

<sup>10</sup>T. He, Y. Wu, G. D'avino, E. Schmidt, M. Stolte, J. Cornil, D. Beljonne, P. P. Ruden, F. Würthner, and C. D. Frisbie, Nat. Commun. 9, 2141 (2018).

<sup>11</sup>B. H. Hamadani, C. A. Richter, D. J. Gundlach, R. J. Kline, I. McCulloch, and M. Heeney, J. Appl. Phys. **102**, 044503 (2007).

<sup>12</sup>A. Bolognesi, M. Berliocchi, M. Manenti, A. DiCarlo, P. Lugli, K. Lmimouni, and C. Dufour, IEEE Trans. Electron Devices 51, 1997 (2004).

<sup>13</sup>T. Minari, T. Nemoto, and S. Isoda, J. Appl. Phys. **99**, 034506 (2006).

<sup>14</sup>S. Cherian, C. Donley, D. Mathine, L. LaRussa, W. Xia, and N. Armstrong, J. Appl. Phys. 96, 5638 (2004).

<sup>15</sup>P. W. M. Blom, M. J. M. de Jong, and M. G. van Munster, Phys. Rev. B 55, R656 (1997).

16T. Kreouzis, D. Poplavskyy, S. Tuladhar, M. Campoy-Quiles, J. Nelson, A. Campbell, and D. Bradley, Phys. Rev. B 73, 235201 (2006).

<sup>17</sup>P. Stallinga, H. L. Gomes, F. Biscarini, M. Murgia, and D. M. De Leeuw, J. Appl. Phys. 96, 5277 (2004).

<sup>18</sup>D. Gupta, N. Jeon, and S. Yoo, Org. Electron. **9**, 1026 (2008).

<sup>19</sup>O. D. Jurchescu, S. Subramanian, R. J. Kline, S. D. Hudson, J. E. Anthony, T. N. Jackson, and D. J. Gundlach, Chem. Mater. 20, 6733 (2008).

- <sup>20</sup>M. R. Niazi, R. Li, E. Q.Li, A. R. Kirmani, M. Abdelsamie, Q. Wang, W. Pan, M. M. Payne, J. E. Anthony, D.-M. Smilgies, S. T. Thoroddsen, E. P. Giannelis, and A. Amassian, Nat. Commun. 6, 8598 (2015).
- <sup>21</sup>R. Hamilton, J. Smith, S. Ogier, M. Heeney, J. E. Anthony, I. McCulloch, J. Veres, D. D. C. Bradley, and T. D. Anthopoulos, Adv. Mater. 21, 1166 (2009).
- <sup>22</sup>Z. A. Lamport, K. J. Barth, H. Lee, E. Gann, S. Engmann, H. Chen, M. Guthold, I. McCulloch, J. E. Anthony, L. J. Richter, D. M. DeLongchamp, and O. D. Jurchescu, Nat. Commun. 9, 5130 (2018).
- <sup>23</sup>J. Panidi, A. F. Paterson, D. Khim, Z. Fei, Y. Han, L. Tsetseris, G. Vourlias, P. A. Patsalas, M. Heeney, and T. D. Anthopoulos, Adv. Sci. 5, 1700290 (2017).
- <sup>24</sup>P. J. Diemer, Z. A. Lamport, Y. Mei, J. W. Ward, K. P. Goetz, W. Li, M. M. Payne, M. Guthold, J. E. Anthony, and O. D. Jurchescu, Appl. Phys. Lett. 107, 103303 (2015).
- <sup>25</sup>Y. Mei, P. J. Diemer, M. R. Niazi, R. K. Hallani, K. Jarolimek, C. S. Day, C. Risko, J. E. Anthony, A. Amassian, and O. D. Jurchescu, Proc. Natl. Acad. Sci. U. S. A. 114, E6739 (2017).
- <sup>26</sup>Y. Mei, D. Fogel, J. Chen, J. W. Ward, M. M. Payne, J. E. Anthony, and O. D. Jurchescu, Org. Electron. 50, 100 (2017).
- <sup>27</sup>J. W. Ward, M. A. Loth, R. J. Kline, M. Coll, C. Ocal, J. E. Anthony, and O. D. Jurchescu, J. Mater. Chem. 22, 19047 (2012).
- <sup>28</sup>Z. A. Lamport, H. F. Haneef, S. Anand, M. Waldrip, and O. D. Jurchescu, J. Appl. Phys. **124**, 071101 (2018).
- <sup>29</sup>J. W. Ward, K. P. Goetz, A. Obaid, M. M. Payne, P. J. Diemer, C. S. Day, J. E. Anthony, and O. D. Jurchescu, Appl. Phys. Lett. **105**, 083305 (2014).
- <sup>30</sup>R. J. Chesterfield, J. C. McKeen, C. R. Newman, P. C. Ewbank, D. A. da Silva Filho, J.-L. Brédas, L. L. Miller, K. R. Mann, and C. D. Frisbie, J. Phys. Chem. B 108, 19281 (2004).
- <sup>31</sup>H. Bässler, Phys. Status Solidi B **175**, 15 (1993).

- <sup>32</sup>S. G. J. Mathijssen, M. Cölle, A. J. G. Mank, M. Kemerink, P. A. Bobbert, and D. M. de Leeuw, Appl. Phys. Lett. **90**, 192104 (2007).
- 33L. Bürgi, H. Sirringhaus, and R. H. Friend, Appl. Phys. Lett. 80, 2913 (2002).
- <sup>34</sup>R. J. Kline, S. D. Hudson, X. Zhang, D. J. Gundlach, A. J. Moad, O. D. Jurchescu, T. N. Jackson, S. Subramanian, J. E. Anthony, M. F. Toney, and L. J. Richter, Chem. Mater. 23, 1194 (2011).
- 35L.-L. Chua, J. Zaumseil, J.-F. Chang, E. C.-W. Ou, P. K.-H. Ho, H. Sirringhaus, and R. H. Friend, Nature 434, 194 (2005).
- <sup>36</sup>I. N. Hulea, S. Fratini, H. Xie, C. L. Mulder, N. N. Iossad, G. Rastelli, S. Ciuchi, and A. F. Morpurgo, Nat. Mater. 5, 982 (2006).
- <sup>37</sup>X. Li, A. Kadashchuk, I. I. Fishchuk, W. T. T. Smaal, G. Gelinck, D. J. Broer, J. Genoe, P. Heremans, and H. Bässler, Phys. Rev. Lett. 108, 066601 (2012).
- <sup>38</sup>S. Hunter, A. D. Mottram, and T. D. Anthopoulos, J. Appl. Phys. **120**, 025502 (2016).
- 39P. J. Diemer, J. Hayes, E. Welchman, R. Hallani, S. J. Pookpanratana, C. A. Hacker, C. A. Richter, J. E. Anthony, T. Thonhauser, and O. D. Jurchescu, Adv. Electron. Mater. 3, 1600294 (2017).
- <sup>40</sup>C.-W. Huang, X. You, P. J. Diemer, A. J. Petty, J. E. Anthony, O. D. Jurchescu, and J. M. Atkin, Commun. Chem. 2, 22 (2019).
- <sup>41</sup>I. I. Fishchuk, A. Kadashchuk, M. Ullah, H. Sitter, A. Pivrikas, J. Genoe, and H. Bässler, Phys. Rev. B 86, 045207 (2012).
- <sup>42</sup>W. F. Pasveer, J. Cottaar, C. Tanase, R. Coehoorn, P. A. Bobbert, P. W. M. Blom, D. M. de Leeuw, and M. A. J. Michels, Phys. Rev. Lett. **94**, 206601
- 43R. Coehoorn, W. F. Pasveer, P. A. Bobbert, and M. A. J. Michels, Phys. Rev. B 72, 155206 (2005).
- <sup>44</sup>C. Liu, G. Li, R. D.Pietro, J. Huang, Y.-Y. Noh, X. Liu, and T. Minari, Phys. Rev. Appl. 8, 034020 (2017).